PHYSICAL REVIEW B **77**, 214429 (2008)

Current-induced domain wall motion in Rashba spin-orbit system

Katsunori Obata[1] and Gen Tatara[1,2]
[1]*Department of Physics, Tokyo Metropolitan University, Hachioji, Tokyo 192-0397, Japan*
[2]*PRESTO, JST, 4-1-8 Honcho Kawaguchi, Saitama 332-0012, Japan*
(Received 1 April 2008; revised manuscript received 23 May 2008; published 23 June 2008)

Current-induced magnetic domain wall motion, induced by transfer of spin transfer effect due to exchange interaction, is expected to be useful for next generation high-density storages. Here we showed that efficient domain wall manipulation can be achieved by the introduction of Rashba spin-orbit interaction, which induces spin precession of conduction electron and acts as an effective magnetic field. Its effect on domain wall motion depends on the wall configuration. We found that the effect is significant for Bloch wall with the hard axis along the current, since the effective field works as β or fieldlike term and removes the threshold current if in extrinsic pinning is absent. For Néel wall and Bloch wall with easy axis perpendicular to Rashba plane, the effective field induces a step motion of wall corresponding to a rotation of wall plane by the angle of approximately π at current lower than intrinsic threshold. Rashba interaction would therefore be useful to assist efficient motion of domain walls at low current.

DOI: 10.1103/PhysRevB.77.214429 PACS number(s): 72.25.Ba, 72.25.Dc

I. INTRODUCTION

In recent years, magnetic-memory devices such as hard disk drives have been utilized for various products such as portable music players and home appliances. With the diversification of the use of these devices, they deal with a much larger amount of information and need to be more miniaturized and to have higher capacity. However, it is believed that the conventional magnetic-memory devices will reach the limit of downsizing and high capacity in the near future. The reason is because the magnetization so far is controlled by a magnetic field and the more miniaturized and the higher capacity they get, the higher necessary field they will need. Therefore, a new method, which replaces the magnetic field, is required. One of the methods expected is the control by electric current, i.e., current-induced magnetization reversal. The current-induced magnetization reversal was pointed out by Berger[1–3] and Slonczeski.[4] The torque is caused by the *s-d* exchange interaction via spin transfer effect arising from conservation of spin angular momentum between the current and the magnetization.

To realize devices using the current-induced magnetization reversal, it is absolutely essential to reduce the current necessary. In this paper, we demonstrate that the problem can be solved by the introduction of Rashba spin-orbit interaction.[5] A spin precession induced by Rashba interaction is expected to affect the spin transfer torque mechanism and to lead to efficient control of magnetization. The interaction has been proposed on two-dimensional electron systems realized at the interface of semiconductors but is now known to arise quite generally when inversion symmetry is broken.[6] For instance, significant Rashba effect can arise on surface of heavy metals.[7,8] Our results therefore would apply to systems of magnetic semiconductors[9] with gate for Rashba interaction attached or on magnetic metallic thin films with heavy ions doped.[8]

Recent theoretical studies revealed that current-driven domain wall motion is significantly affected by spin-relaxation process. Actually, spin-relaxation triggers a torque perpendicular to the adiabatic spin transfer torque,[10,11] and this torque, β torque,[11] acts as an effective force on domain wall, which deletes intrinsic pinning effects.[11,12] Microscopic analysis of spin relaxation was done in the case of spin-flip scattering by random impurity spins and value of β was found to be of similar magnitude with (but not necessarily equal to) the spin-relaxation contribution to Gilbert damping parameter α (Refs. 13–16). On the other hand, role of spin-orbit interaction, which also causes spin relaxation, on the wall dynamics has not been much studied so far. Spin-orbit interaction in magnetic semiconductors was recently studied based on Kohn-Luttinger Hamiltonian, and large enhancement of wall velocity due to spin-orbit interaction was found.[17] The Rashba spin-orbit interaction we are going to study here turns out also to assist wall motion to a large extent.

Experimentally, existence of spin-relaxation induced torque (β term) is indicated in metallic systems.[18,19] In fact, the domain velocities observed in Refs. 18 and 19 were explained by a rigid wall theory if finite β is taken into account of. The magnitude found there was $\beta \sim O(\alpha)$ (Ref. 19) and $\beta \sim 8\alpha$ (Ref. 18), where α is Gilbert damping parameter.

In magnetic semiconductors, domain wall motion induced by current have been observed.[20–22] The threshold current and wall velocity at high current was in agreement with purely spin transfer induced motion of a rigid wall.[21] This fact suggests that strong spin-orbit interaction acting in semiconductors does not induce β term. Absence or negligibly small β terms in semiconductor was confirmed in the creep regime, too.[22] In fact, the critical exponent of wall velocity under current was found to be different from that under the magnetic field, indicating clearly that β term, which acts as an external magnetic field, does not play essential role in the current-driven creep motion.

In this paper, we study current-driven domain wall motion in the presence of Rashba interaction. Rashba interaction acts on x-y plane and electric current is applied along x axis. The spin system we consider is with easy and hard axes. The wall is treated as planar and rigid, which is justified if easy axis

energy gain, K, is larger than hard axis anisotropy energy, $K_\perp$.[23–25] We consider three cases where easy axis direction (we call η) is x, y, and z. The wall structure in these three cases are Néel for $\eta=x$ and Bloch wall for $\eta=y,z$. We will see that dynamics of Néel wall and Bloch wall with $\eta=z$ [called Bloch(z)] are essentially the same, while Bloch with $\eta=y$ [Bloch(y)] is different. The effect of current is calculated for each anisotropy configuration using gauge transformation in spin space, assuming adiabatic limit. The Rashba interaction is treated perturbatively to the second order. Expansion with respect to Rashba interaction is justified here since electron has large spin polarization Δ. (This is in contrast to the spin Hall case without polarization, where perturbative treatment is not allowed.[26])

We will see that the most important effect of Rashba interaction is to induce effective magnetic field perpendicular to both the current (along x direction) and to the Rashba field (chosen as perpendicular to the xy plane), namely, in the y direction. In the case of Bloch wall with easy axis along the y direction, the effective field is along the easy axis and acts as a β term. The magnitude of induced β is estimated to be quite large, $\beta/\alpha \sim 10$ for realistic semiconductors. The intrinsic threshold is removed by this β and the wall speed is greatly enhanced.

In the case of Néel wall and Bloch wall with easy axis perpendicular to the plane, the effective field is perpendicular to the easy axis. This field induces a potential for ϕ (angle of wall magnetization), which breaks the periodicity of π due to standard second-order magnetic anisotropies. The field therefore lowers half of the local energy barriers in the space of ϕ but increases the other half of the local energy barriers. This results at low current in a step motion of the wall over a distance $\Delta X \simeq \pi\ell/\alpha$, where ℓ is the wall thickness, corresponding to a shift of $\Delta\phi \sim \pi$. This motion occurs below intrinsic threshold, and the distance ΔX can be quite large, and could be useful for applications.

The domain wall motion in Rashba system would be realized in magnetic semiconductors with a gate controlling Rashba interaction. Another exciting possibility is to use surface or thin film of metals. In the case of nonmagnetic metals such as Au or Ag doped with Bi, a very strong Rashba interaction (corresponding to 5–40 times larger than conventional Rashba interaction in semiconductors) has been found on the surfaces.[7,8] If such strong Rashba interaction is realized also in magnetic metals, the domain wall motion there would be very different from and much more efficient than those observed so far.

Below, we will derive the effective Hamiltonian for local spin, we will also derive the equation of motion for domain wall, and then we will discuss wall dynamics by solving the equation. Those who are not interested in technical details can skip to Sec. VII or Sec. VIII.

II. MODEL AND METHOD

A. Local spin

Domain wall is described by a Lagrangian of local spins given by

TABLE I. Configuration of magnetic anisotropy and corresponding domain wall structure.

	Easy (η) axis (K)	Hard axis ($K_\perp$)
Bloch(z)	z	y
Néel(x)	x	z
Bloch(y)	y	x

$$L_s = \int \frac{d^3x}{a^3}\hbar S(\cos\theta - 1) - H_s, \tag{1}$$

where local spin direction is expressed by polar coordinates (θ,ϕ). The first term describes time evolution of local spin (spin Berry phase term). The Hamiltonian of local spin we considered is given as follows:

$$H_s = \int \frac{d^3x}{a^3}\left[\frac{J}{2}(\nabla S)^2 - \frac{K}{2}(S_\parallel)^2 + \frac{K_\perp}{2}(S_\perp)^2\right]. \tag{2}$$

The first term is a ferromagnetic exchange interaction between local spins, the second and third terms are magnetic anisotropy energies. $S_\parallel$ is the easy axis component of spin and $K(>0)$ is the corresponding anisotropic energy, and $S_\perp$ and $K_\perp$ are hard axes ones.

In the absence of Rashba interaction, we can choose space coordinate and spin coordinate independently. When the Rashba spin-orbit interaction is switched, spin and space coordinates correlate each other, and the spin torque and gauge field depend on the choice of magnetic easy axis, which we call η axis. We consider three different cases with easy axis $\eta=x$, y, and z. Domain wall structure then becomes Néel and Bloch walls. We will call the domain wall configuration with the easy axis label, such as Bloch(z) for a Bloch wall with $\eta=z$ (see Table I).

In this paper Rashba interaction acts within xy plane and current is applied always along x. Instead, our definition of polar angle in spin space depends on the wall configuration. We define θ as the angle measured from the easy axis (i.e., $S_\parallel=\cos\theta$), and ϕ as the angle in the plane perpendicular to easy axis. The hard axis is given by $\phi=\frac{\pi}{2}$ and so the hard axis component is written as $S_\perp=\sin\theta\sin\phi$. Note therefore that (θ,ϕ) for Néel and Bloch(y) walls below are different from standard definition measured from z axis. Lagrangian L_s is thus written in terms of polar angle as

$$L_s = \int \frac{d^3x}{a^3}\left\{\hbar S\dot{\phi}(\cos\phi - 1) - \frac{J}{2}[(\nabla\theta)^2 + \sin^2\theta(\nabla\phi)^2] - \frac{KS^2}{2}\sin^2\theta - \frac{K_\perp S^2}{2}\sin^2\theta\sin^2\phi\right\}, \tag{3}$$

for any type of walls considered here.

B. Conduction electron

The Hamiltonian of the conduction electron is given by the following four terms: The first term is the free-electron part represented as

$$H_e = \int d^3x c^\dagger(x)\left[-\frac{\hbar^2}{2m}\nabla^2 - \varepsilon_F\right]c(x), \tag{4}$$

where c and $c^\dagger$ are electron annihilation and creation operators, ε_F is the Fermi energy, and m is the effective mass. The second is the exchange interaction between electron and local spin,

$$H_{\rm ex} = -\frac{\Delta}{S}\int d^3x \boldsymbol{S}\cdot[c^\dagger(x)\boldsymbol{\sigma}c(x)], \tag{5}$$

where Δ is the magnitude of the interaction, $\boldsymbol{S}$ is the local spin vector, and $\boldsymbol{\sigma}$ are Pauli matrices. The third one, the Rashba spin-orbit interaction, is given as

$$H_{\rm so} = \frac{i\lambda}{2}\int d^3x c^\dagger(x)[(\overleftrightarrow{\nabla}_x\sigma^y - \overleftrightarrow{\nabla}_y\sigma^x)]c(x), \tag{6}$$

where $\overleftrightarrow{\nabla}$ acts on both sides and λ is the magnitude of the Rashba interaction (the dimensions are $[J\cdot m]$). When electric field is applied in the x direction, the momentum, $-i\hbar\langle c^\dagger(x)\nabla_x c(x)\rangle$, grows and the Rashba interaction then changes the electron-spin direction toward y direction, inducing electron-spin precession.

Since we are interested in a response of local spins to applied current, we introduce the interaction with electric field, given by [neglecting $O(E^2)$]

$$H_{\rm EM} = -e\int d^3x \boldsymbol{A}_{\rm EM}\cdot[c^\dagger(x)\boldsymbol{v}c(x)], \tag{7}$$

where $\boldsymbol{A}_{\rm EM}=\frac{\boldsymbol{E}}{i\Omega}e^{i\Omega t}$ is a $U(1)$ gauge field and $\boldsymbol{E}$ is applied electric field. Velocity operator is given as

$$v_\nu = \frac{-i\hbar\nabla_\nu}{m} + \frac{\lambda}{\hbar}(\delta_{\nu,y}\sigma^x - \delta_{\nu,x}\sigma^y). \tag{8}$$

The field $\boldsymbol{E}$ is spatially uniform but has finite frequency Ω. This frequency is introduced for calculation purpose and is chosen as $\Omega=0$ at the end of calculation, as is usually the case of linear-response calculation.

C. Gauge transformation

The exchange interaction, $H_{\rm ex}$, has in general off-diagonal components. Besides the local ground state of conduction electron varies at each lattice point if magnetization is nonuniform. In this case, local gauge transformation in spin space,[27,28] which diagonalizes the exchange interaction, is useful. The spatial change of local spin is then represented by a gauge field, which is proportional to spatial spin variation, $\partial_\mu \boldsymbol{S}$. We consider the case when local spin profile is slowly varying (called the adiabatic limit), and then gauge field is small. We thus examine only the first-order contribution of gauge field. A new electron operator, a, after gauge transformation is defined by the use of 2×2 unitary matrix U as

$$c(x) = U(x)a(x), \tag{9}$$

where electron operators here have two spin components such as $c\equiv(c_+,c_-)$. The matrix U is expressed using Pauli matrix as

$$U(x) = \boldsymbol{m}(x)\cdot\boldsymbol{\sigma}, \tag{10}$$

where $\boldsymbol{m}(x)$ is a vector, which characterizes the gauge transformation. We denote the spin easy axis as η (e.g., $\eta=x$ for Néel wall). The gauge transformation is defined so that conduction-electron spins are polarized along magnetic easy axis η, i.e., to satisfy $\frac{\mathbf{S}(x)}{S}\cdot[c^\dagger(x)\boldsymbol{\sigma}c(x)]=a^\dagger(x)\sigma^\eta a(x)$. (The transformation thus differs for different wall configuration.) The Hamiltonian given by Eqs. (4)–(6) is written in a-electron representation as

$$\begin{aligned} H_e + H_{\rm ex} + H_{\rm so} = \int d^3x\Bigg\{ & a^\dagger\Bigg[-\frac{\hbar^2}{2m}\nabla^2 - \Delta\sigma^\eta - i\lambda(\sigma^y\nabla_x \\ & - \sigma^x\nabla_y)\Bigg]a - \frac{i\hbar^2}{m}A^\alpha_\mu a^\dagger\sigma^\alpha\nabla_\mu a + \lambda(A^y_x \\ & - A^x_y)a^\dagger a + 2i\lambda[m^y m^\beta a^\dagger\sigma^\beta\nabla_x a \\ & - m^x m^\beta a^\dagger\sigma^\beta\nabla_y a]\Bigg\},. \end{aligned} \tag{11}$$

where gauge field is given as

$$A_\mu \equiv -iU^\dagger\nabla_\mu U = (\boldsymbol{m}\times\partial_\mu\boldsymbol{m})\cdot\boldsymbol{\sigma} \equiv A^\alpha_\mu\sigma^\alpha. \tag{12}$$

The electromagnetic interaction after gauge transformation is given as

$$H_{\rm EM} = \int d^3x \frac{-eE_x}{i\Omega}a^\dagger\left[\frac{-i\hbar\nabla_x}{m} + \frac{\hbar}{m}A_x - \frac{\lambda}{\hbar}\overline{\sigma^y}\right]a, \tag{13}$$

where $\overline{\sigma^\mu}\equiv U^\dagger\sigma^\mu U = 2m^\mu(\boldsymbol{m}\cdot\boldsymbol{\sigma}) - \sigma^\mu$ and the electric field is applied in x direction.

The total electron Hamiltonian is therefore obtained as

$$\begin{aligned} H = \int d^3x\Bigg\{ & a^\dagger\Bigg[-\frac{\hbar^2}{2m}\nabla^2 - \Delta\sigma^\eta - i\lambda(\sigma^y\nabla_x - \sigma^x\nabla_y) \\ & + \frac{eE_x}{\Omega}\left(\frac{\hbar\nabla_x}{m} - \frac{\lambda}{i\hbar}\sigma^y\right)\Bigg]a - \frac{i\hbar^2}{m}A^\alpha_\mu a^\dagger\sigma^\alpha\nabla_\mu a + \lambda(A^y_x \\ & - A^x_y)a^\dagger a + 2i\lambda[m^y m^\beta a^\dagger\sigma^\beta\nabla_x a - m^x m^\beta a^\dagger\sigma^\beta\nabla_y a] \\ & - \frac{eE_x}{i\Omega}a^\dagger\left[\frac{\hbar}{m}A^\alpha_x\sigma^\alpha - \frac{2\lambda}{\hbar}m^y(\boldsymbol{m}\cdot\boldsymbol{\sigma})\right]a\Bigg\}. \end{aligned} \tag{14}$$

D. Effective Hamiltonian

The current-induced part of the effective Hamiltonian for local spin is directly obtained from Eq. (14) as

$$\begin{aligned} H_{\rm eff} = \int d^3x\Bigg\{ & \hbar A^\alpha_\mu j^\alpha_{s,\mu} + \lambda n(A^y_x - A^x_y) - \frac{2m}{\hbar}\lambda[m^y m^\beta j^\beta_{s,x} \\ & - m^x m^\beta j^\beta_{s,y}] - \frac{eE_x}{i\Omega}\left[\frac{\hbar}{m}A^\alpha_x s^\alpha - \frac{2\lambda}{\hbar}m^y m^\alpha s^\alpha\right]\Bigg\}, \end{aligned} \tag{15}$$

where electron properties are represented by the following expectation values:

$$n(x) \equiv \langle a^\dagger(x)a(x)\rangle, \tag{16}$$

$$s^\alpha(x) \equiv \langle a^\dagger(x)\sigma^\alpha a(x)\rangle, \tag{17}$$

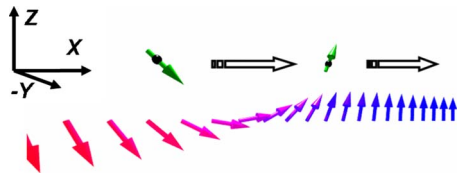

FIG. 1. (Color online) Bloch(z) wall configuration with easy axis along z direction and hard axis along y axis. The spin of incoming electron is schematically shown.

$$j^{\alpha}_{s,\mu}(x) \equiv -\frac{i\hbar}{2m}\langle a^{\dagger}(x)\overleftrightarrow{\nabla}_{\mu}\sigma^{\alpha}a(x)\rangle. \tag{18}$$

Here $\langle\ \rangle$ denotes expectation value evaluated using nonperturbed Hamiltonian H_a defined as

$$H_a \equiv \int d^3x a^{\dagger}(x)\left[-\frac{\hbar^2}{2m}\nabla^2 - \Delta\sigma^{\eta} - i\lambda(\sigma^y\nabla_x - \sigma^x\nabla_y)\right]a(x), \tag{19}$$

and including to linear order, the effect of current,

$$H^0_{\mathrm{EM}} \equiv \int d^3x a^{\dagger}(x)\left[\frac{eE_x}{\Omega}\left(\frac{\hbar\nabla_x}{m} - \frac{\lambda}{i\hbar}\sigma^y\right)\right]a(x). \tag{20}$$

Current-induced part of the effective Lagrangian is given by

$$L_{\mathrm{eff}} = \int d^3x[\hbar A^{\alpha}_t s^{\alpha}] - H_{\mathrm{eff}}. \tag{21}$$

In calculating the expectation values, the Rashba spin-orbit interaction is treated perturbatively to the second-order, λ^2. This approximation corresponds to assuming $\frac{\lambda k_f}{\varepsilon_F} \ll 1$ with Fermi wave vector k_F. This expansion with respect to λ is justified by the presence of Δ, in contrast to the nonperturbative nature of unpolarized Rashba system.[26] We also assume that the effect of impurities is weak and the electron lifetime is long, i.e., $\frac{1}{\varepsilon_F\tau} \ll 1$. In this case, the term in Eq. (15) including electric field turns out to be small by a factor of $\frac{1}{\varepsilon_F\tau}$ compared with dominant contributions. We will thus evaluate the effective Hamiltonian given by

$$H_{\mathrm{eff}} = \int d^3x\left\{\hbar A^{\alpha}_{\mu} j^{\alpha}_{s,\mu} + \lambda n(A^y_x - A^x_y) - \frac{2m}{\hbar}\lambda[m^y m^{\beta} j^{\beta}_{s,x} - m^x m^{\beta} j^{\beta}_{s,y}]\right\}. \tag{22}$$

III. BLOCH(z) CASE

In this section, we derive the effective Hamiltonian for the anisotropy configuration of Bloch(z) type, namely, magnetic easy axis is in the z direction and hard axis is in the y direction.

In this case, domain wall configuration is Bloch(z) wall shown in Fig. 1. Polar coordinates are defined by (as in Fig. 2)

$$\boldsymbol{S}(x,t) = S(\sin\theta\cos\phi, \sin\theta\sin\phi, \cos\theta). \tag{23}$$

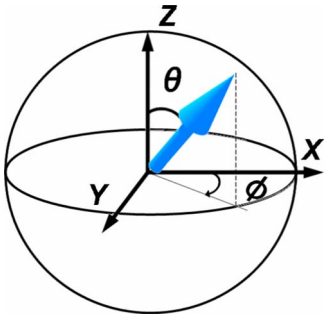

FIG. 2. (Color online) Polar coordinates of local spin in the Bloch(z) case.

In the case of Bloch(z)-type anisotropy, the gauge transformation is defined by $\boldsymbol{S}(U^{\dagger}\boldsymbol{\sigma}U) = S\sigma^z$. This is satisfied by choosing

$$\boldsymbol{m} = \left(\sin\frac{\theta}{2}\sin\phi, \cos\frac{\theta}{2}, \sin\frac{\theta}{2}\cos\phi\right). \tag{24}$$

Gauge field is then given as

$$A_{\mu} = \begin{pmatrix} A^x_{\mu} \\ A^y_{\mu} \\ A^z_{\mu} \end{pmatrix} = \frac{1}{2}\begin{pmatrix} -\partial_{\mu}\theta\sin\phi - \sin\theta\cos\phi\partial_{\mu}\phi \\ \partial_{\mu}\theta\cos\phi - \sin\theta\sin\phi\partial_{\mu}\phi \\ (1-\cos\theta)\partial_{\mu}\phi \end{pmatrix}. \tag{25}$$

The unperturbed Hamiltonian, given by choosing $\eta = z$ in Eq. (19), reads as

$$H_a = \int d^3x a^{\dagger}(x)\left[-\frac{\hbar^2}{2m}\nabla^2 - \Delta\sigma^z - i\lambda(\sigma^y\nabla_x - \sigma^x\nabla_y)\right]a(x). \tag{26}$$

This Hamiltonian H_a has the off-diagonal elements in the spin space due to Rashba interaction, and so we will diagonalize it using a unitary transformation in momentum space, $a^{\dagger}_{\boldsymbol{k}} = d^{\dagger}_k T^{\dagger}_k$, where $d^{\dagger}_k$ is a new creation operator and T_k is a 2×2 unitary matrix. The Hamiltonian H_a in momentum space reads as

$$H_a = \sum_k d^{\dagger}_k T^{\dagger}_k \begin{pmatrix} \varepsilon_{\boldsymbol{k}} - \Delta & -i\lambda k_- \\ i\lambda k_+ & \varepsilon_{\boldsymbol{k}} - \Delta \end{pmatrix} T_k d_k, \tag{27}$$

where $k_{\pm} \equiv k_x \pm ik_y$. Diagonalization of H_a is done by choosing the unitary matrix T_k as

$$T_k \equiv \frac{1}{\sqrt{A^2_k + \lambda^2 k^2}}\begin{pmatrix} A_k & i\lambda k_- \\ -i\lambda k_+ & -A_k \end{pmatrix}, \tag{28}$$

where $A_k = \Delta + Z_k, Z_k = \sqrt{\Delta^2 + \lambda^2 k^2}$. The result is

$$H_a = \sum_k d^{\dagger}_k \begin{pmatrix} \varepsilon_{\boldsymbol{k}} - Z_k & 0 \\ 0 & \varepsilon_{\boldsymbol{k}} + Z_k \end{pmatrix} d_k. \tag{29}$$

After diagonalization, the energy of conduction electrons is spin split as

$$\varepsilon_{k,\sigma} = \frac{\hbar k^2}{2m} - \varepsilon_F - \sigma Z(k), \tag{30}$$

where $\sigma = (+,-)$ is the spin polarization.

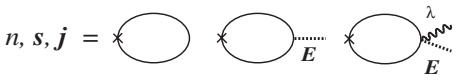

FIG. 3. Diagrammatic representation of electron density (n), spin density (s^α), and spin current ($j^\alpha_{s,i}$) at the linear order in the applied electric field, $\boldsymbol{E}$. Solid line represents electron Green's function with Rashba interaction included. Vertex denoted by $\times$ is 1, σ^α, and $k_i\sigma^\alpha$ for n, s^α, and $j^\alpha_{s,i}$, respectively.

Now, let us estimate the expectation values. The electron density n (Fig. 3) is given as

$$n = -\sum_{k,\omega} i\mathrm{Tr}[\tilde{G}_{k,\omega}]^< + \lim_{\Omega\to 0}\sum_{k,\omega}\frac{eE_x}{\Omega}\frac{\hbar^2 k_x}{m}\mathrm{Tr}[\tilde{G}_{k,\omega}\tilde{G}_{k,\omega+\Omega}]^< + \lim_{\Omega\to 0}\sum_{k,\omega}\frac{eE_x}{\Omega}\lambda\ \mathrm{Tr}[\tilde{G}_{k,\omega}\tilde{\sigma}^y\tilde{G}_{k,\omega+\Omega}]^<, \tag{31}$$

where Tr is a trace in spin space and $\tilde{\sigma}^\alpha \equiv T_k^\dagger \sigma^\alpha T_k$. Keldysh Green's function[29,30] with Rashba interaction included, $\tilde{G}^<_{k,\omega}$, is defined as

$$\tilde{G}^<_{k,\omega} \equiv i\langle d^\dagger_{k,\omega} d_{k,\omega}\rangle = \begin{pmatrix} g^<_{k,\omega,\uparrow} & 0 \\ 0 & \tilde{g}^<_{k,\omega,\downarrow} \end{pmatrix}, \tag{32}$$

where component $\tilde{g}^<_{k,k,\omega,\sigma}$ is given as

$$\tilde{g}^<_{k,\omega,\sigma} = 2\pi i f(\omega)\delta(\hbar\omega - \varepsilon_{k,\sigma}), \tag{33}$$

$f(\omega) \equiv \frac{1}{e^{\beta\omega}+1}$ being the Fermi distribution function (β is inverse temperature). Summation over k is carried out in two-dimensions by replacing by energy integration, $\Sigma_k = \frac{Vm}{2\pi\hbar^2}\int d\varepsilon$. Products of Keldysh Green's functions is calculated using relations,

$$\tilde{G}^<_{k,\omega} \equiv f(\omega)[\tilde{G}^a_{k,\omega} - \tilde{G}^r_{k,\omega}], \tag{34}$$

where $\tilde{G}^r_{k,\omega}$ ($\tilde{G}^a_{k,\omega}$) is retarded (advanced) Green's function, and

$$\begin{aligned}[G_{k,\omega}G_{k',\omega+\Omega}]^< &= G^r_{k,\omega}G^<_{k',\omega+\Omega} + G^<_{k,\omega}G^a_{k',\omega+\Omega} \\ &= G^r_{k,\omega}G^a_{k',\omega+\Omega}[f(\omega+\Omega) - f(\omega)] \\ &\quad - G^r_{k,\omega}G^r_{k',\omega+\Omega} + G^a_{k,\omega}G^a_{k',\omega+\Omega}.\end{aligned} \tag{35}$$

Expanding with respect to λ to the second order, we obtain the density as

$$n = \frac{m}{\pi\hbar^2}\varepsilon_F + \frac{m^2\lambda^2}{\pi\hbar^4}. \tag{36}$$

We see that there is no effect from the applied electric field here.

The electron-spin density s^γ is similarly calculated as

$$\begin{aligned}s^\gamma &= -\sum_{k,\omega} i\ \mathrm{Tr}[\tilde{\sigma}^\gamma\tilde{G}_{k,\omega}]^< \\ &\quad + \lim_{\Omega\to 0}\sum_{k,\omega}\frac{eE_x\hbar^2 k_x}{\Omega m}\mathrm{Tr}[\tilde{\sigma}^\gamma\tilde{G}_{k,\omega}\tilde{G}_{k,\omega+\Omega}]^< \\ &\quad + \lim_{\Omega\to 0}\sum_{k,\omega}\frac{eE_x\lambda}{\Omega}\mathrm{Tr}[\tilde{\sigma}^\gamma\tilde{G}_{k,\omega}\tilde{\sigma}^y\tilde{G}_{k,\omega+\Omega}]^<.\end{aligned} \tag{37}$$

The result is

$$s^x = -\frac{meE_x\lambda}{2\pi\hbar^2\Delta},$$

$$s^y = \frac{meE_x\tau\lambda}{\pi\hbar^2},$$

$$s^z = \frac{m\Delta}{\pi\hbar^2}. \tag{38}$$

We see that the electric field induces perpendicular components s^x and s^y, but $|s^y| \gg |s^x|$ since $\frac{1}{\Delta\tau} \ll 1$. We will thus approximate $|s^x| \simeq 0$. The z component of spin in Eq. (38) is the adiabatic contribution, which is not affected by applied field.

Spin current, $j^\alpha_{s,\mu}$, is estimated using,

$$\begin{aligned}i\langle a^\dagger_{\boldsymbol{k}} k_\mu \sigma^\alpha a_{\boldsymbol{k}}\rangle &= \sum_{k,\omega} k_\mu\ \mathrm{Tr}[\tilde{\sigma}^\alpha\tilde{G}_{k,\omega}]^< \\ &\quad - \lim_{\Omega\to 0}\sum_{k,\omega} k_\mu\frac{eE_x\hbar^2 k_x}{i\Omega m}\mathrm{Tr}[\tilde{\sigma}^\alpha\tilde{G}_{k,\omega}\tilde{G}_{k,\omega+\Omega}]^< \\ &\quad - \lim_{\Omega\to 0}\sum_{k,\omega} k_\mu\frac{eE_x\lambda}{i\Omega}\mathrm{Tr}[\tilde{\sigma}^\alpha\tilde{G}_{k,\omega}\tilde{\sigma}^y\tilde{G}_{k,\omega+\Omega}]^<,\end{aligned} \tag{39}$$

as

$$j^x_{s,y} = \frac{m}{\pi\hbar^3}\lambda\varepsilon_F,$$

$$j^y_{s,x} = -\frac{m}{\pi\hbar^3}\lambda\varepsilon_F,$$

$$j^z_{s,x} = -\frac{eE_x\tau}{\pi\hbar}\left[\Delta - \frac{m\lambda^2}{2\Delta\hbar^2}\varepsilon_F\right]. \tag{40}$$

We see that spin current are generated in x and y direction by the Rashba interaction without electric field and that $j^x_{s,y}$ is equal to $-j^y_{s,x}$. This is due to the symmetry of the Rashba spin-orbit interaction. In contrast, $j^z_{s,x}$ is induced by applied electric field. We define the current density (divided by e) and electron density without spin-orbit interaction as (σ is Boltzmann conductivity)

$$J \equiv -\frac{eE_x\tau\varepsilon_F}{\pi\hbar} = \frac{\sigma}{e}E_x, \tag{41}$$

and

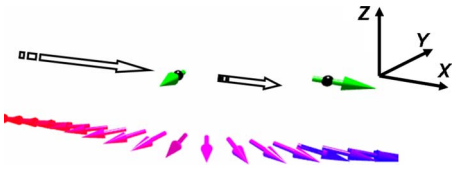

FIG. 4. (Color online) Néel(x) wall configuration.

$$n_0 \equiv \frac{\varepsilon_F m}{\pi\hbar^2}. \tag{42}$$

In terms of these parameters, the above result reads

$$n = n_0\left[1 + \frac{m\lambda^2}{2\hbar^2\varepsilon_F}\right],$$

$$(s^x, s^y, s^z) = \left(0, -\frac{m\lambda}{\hbar\varepsilon_F}J, n_0\frac{\Delta}{\varepsilon_F}\right),$$

$$(j^y_{s,x}, j^z_{s,x}, j^x_{s,y}) = \left[-\frac{\lambda}{\hbar}n_0, \left(\frac{\Delta}{\varepsilon_F} - \frac{m\lambda^2}{2\Delta\hbar^2}\right)J, \frac{\lambda}{\hbar}n_0\right]. \tag{43}$$

Other components of spin current vanish.

The effective Hamiltonian for Bloch(z) case is therefore obtained from Eq. (22) as

$$H_{\text{eff}} = \int d^3x\left[\frac{\hbar}{2}(1-\cos\theta)(\partial_x\phi)j^z_{s,x} - \frac{\lambda m}{\hbar}[j^z_{s,x}\sin\theta\sin\phi + (1-\cos\theta)(j^y_{s,x} - \sin\phi j^x_{s,y})]\right]. \tag{44}$$

We see that applied current induces $j^z_{s,x}$ [Eq. (43)], and this is induced when coupled with Rashba interaction, an effective magnetic field in y direction as indicated by the second term. The first term of Eq. (44) represents standard spin transfer torque (with current modified by Rashba interaction). The third term is independent of applied current and is a modification of magnetic anisotropy by Rashba interaction.

IV. NÉEL(x) CASE

In this section, we consider a case of Néel wall realized when magnetic easy and hard axes are in the x and z direction, respectively (Fig. 4). Polar coordinates are defined differently from standard definition as (Fig. 5)

$$\boldsymbol{S} = S(\cos\theta, \sin\theta\cos\phi, \sin\theta\sin\phi). \tag{45}$$

Derivation of effective Hamiltonian is done similarly to Bloch(z) case. Difference is in definition of gauge transformation, $\boldsymbol{S}(U^\dagger\boldsymbol{\sigma}U) = S\sigma^x$. Vector $\boldsymbol{m}$ is accordingly chosen as

$$\boldsymbol{m} = \left(\cos\frac{\theta}{2}, \sin\frac{\theta}{2}\cos\phi, \sin\frac{\theta}{2}\sin\phi\right), \tag{46}$$

and A^α_μ is given as

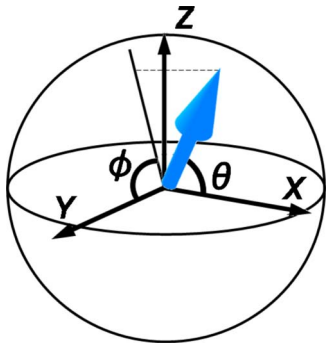

FIG. 5. (Color online) Definition of polar coordinates for Néel(x) case.

$$A_\mu = \frac{1}{2}\begin{pmatrix} (1-\cos\theta)\partial_\mu\phi \\ -\sin\phi\partial_\mu\theta - \sin\theta\cos\phi\partial_\mu\phi \\ \partial_\mu\theta\cos\phi - \sin\theta\sin\phi\partial_\mu\phi \end{pmatrix}. \tag{47}$$

Hamiltonian H_a is also different from Bloch(z) case since uniform spin polarization is now along x direction. It is given as

$$H_a = \sum_k a^\dagger_{\boldsymbol{k}}\begin{pmatrix} \varepsilon_{\boldsymbol{k}} & -b_- \\ -b_+ & \varepsilon_{\boldsymbol{k}} \end{pmatrix}a_{\boldsymbol{k}}, \tag{48}$$

where $b_\pm \equiv (\Delta \mp i\lambda k_\pm)$. The diagonalization of H_a is carried out as $a^{\frac{\dagger}{\dagger}}_{\boldsymbol{k}} = d^\dagger_k T^\dagger_k$, where

$$T \equiv \frac{1}{\sqrt{2}Z_k}\begin{pmatrix} Z_k & b_- \\ b_+ & -Z_k \end{pmatrix}, \tag{49}$$

where

$$Z_k = \sqrt{\Delta^2 + 2\lambda\Delta k_y + \lambda^2 k^2}. \tag{50}$$

The Hamiltonian after diagonalization reads

$$H_a = \sum_k d^\dagger_k\begin{pmatrix} \varepsilon_{\boldsymbol{k}} - Z_k & 0 \\ 0 & \varepsilon_{\boldsymbol{k}} + Z_k \end{pmatrix}d_k. \tag{51}$$

The expectation values are calculated similarly to Bloch(z) case and we obtain,

$$n = n_0, \tag{52}$$

$$(s^x, s^y) = \left[n_0\left(\frac{\Delta}{\varepsilon_F} - \frac{\lambda^2}{2\Delta}\right), -\frac{m\lambda}{\varepsilon_F\hbar}J\right] \tag{53}$$

$$(j^x_{s,x}, j^y_{s,x}, j^x_{s,y}) = \left(\frac{\Delta}{\varepsilon_F}J, -\frac{\lambda}{\hbar}n_0, \frac{\lambda}{\hbar}n_0\right), \tag{54}$$

where other components of spin and spin current vanish.

The current-induced effective Hamiltonian is then obtained as

$$H_{\text{eff}} = \int d^3x\frac{\hbar}{2}(1-\cos\theta)(\partial_x\phi)j^x_{s,x} - \frac{m}{\hbar}\lambda[j^x_{s,x}\sin\theta\cos\phi + (1-\cos\theta)(j^y_{s,x}\cos^2\phi - j^x_{s,y})]. \tag{55}$$

The applied current coupled with spin-orbit interaction in-

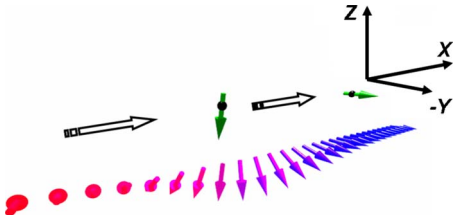

FIG. 6. (Color online) Bloch(y) wall configuration.

duces an effective magnetic field along hard, i.e., y axis [second term of Eq. (55)], as in the Bloch(z) case.

V. BLOCH(y) CASE

Finally, we consider a case of magnetic easy and hard axes along y and x directions, respectively. Domain wall in this case is Bloch(y) wall (Fig. 6). Polar coordinates are define as (Fig. 7)

$$\boldsymbol{S} = S(\sin\theta\sin\phi, \cos\theta, \sin\theta\cos\phi). \tag{56}$$

Gauge transformation is given by $\boldsymbol{S}(U^\dagger \boldsymbol{\sigma} U) = S\sigma^y$, and vector $\boldsymbol{m}$ consequently becomes

$$\boldsymbol{m} = \left(\sin\frac{\theta}{2}\sin\phi, \cos\frac{\theta}{2}, \sin\frac{\theta}{2}\cos\phi\right), \tag{57}$$

and gauge field is

$$A_\mu = \frac{1}{2}\begin{pmatrix} \partial_\mu\theta\cos\phi - \sin\theta\sin\phi\partial_\mu\phi \\ (1-\cos\theta)\partial_\mu\phi \\ -\sin\phi\partial_\mu\theta - \sin\theta\cos\phi\partial_\mu\phi \end{pmatrix}. \tag{58}$$

Hamiltonian H_a is given as

$$H_a = \sum_k a_{\boldsymbol{k}}^\dagger \begin{pmatrix} \varepsilon_{\boldsymbol{k}} & -ib_- \\ -ib_+ & \varepsilon_{\boldsymbol{k}} \end{pmatrix} a_{\boldsymbol{k}}, \tag{59}$$

where $b_\pm = (\Delta \mp \lambda k_\pm)$ (is different from the Néel case). Hamiltonian H_a is diagonalized as

$$H_a = \sum_k d_k^\dagger \begin{pmatrix} \varepsilon_{\boldsymbol{k}} - Z_k & 0 \\ 0 & \varepsilon_{\boldsymbol{k}} + Z_k \end{pmatrix} d_k, \tag{60}$$

by defining $a_{\boldsymbol{k}}^\dagger = d^\dagger T_k^\dagger$ with

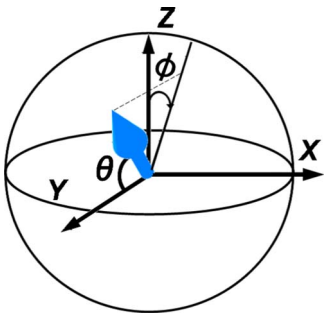

FIG. 7. (Color online) Polar coordinates for Bloch(y) configuration.

$$T \equiv \frac{1}{\sqrt{2}Z_k}\begin{pmatrix} -Z_k & ib_- \\ -ib_+ & Z_k \end{pmatrix}, \tag{61}$$

where

$$Z_k \equiv \sqrt{\Delta^2 - 2\lambda\Delta k_x + \lambda^2 k^2}. \tag{62}$$

Expectation values, which appears in the effective Hamiltonian, are estimated as

$$n = n_0\left[1 - \frac{3m}{\varepsilon_F\hbar^2}\lambda^2\right],$$

$$s^y = n_0\left[\frac{\Delta}{\varepsilon_F} + \frac{m\lambda^2}{\Delta\hbar^2}\right]\lambda J,$$

$$(j_{s,x}^y, j_{s,y}^x) = \left[-n_0\frac{\lambda}{\hbar} + J\left(\frac{\Delta}{\varepsilon_F} + \frac{m\lambda^2}{\varepsilon_F\hbar^2} + \frac{2m\lambda^2}{\Delta\hbar^2}\right), n_0\frac{\lambda}{\hbar} - \frac{m\lambda^2}{\Delta\hbar^2}J\right]. \tag{63}$$

The effective Hamiltonian is therefore obtained as

$$H_{\text{eff}} = \int d^3x\left\{\frac{1}{2}(1-\cos\theta)(\partial_x\phi)[\hbar j_{s,x}^y + \lambda n] - \frac{m\lambda}{\hbar}[(1+\cos\theta)j_{s,x}^y - (1-\cos\theta)j_{s,y}^x\sin^2\phi]\right\}. \tag{64}$$

VI. ANALYSIS OF EFFECTIVE HAMILTONIAN

The effective Hamiltonian representing the effect of current obtained above is summarized as follows;

Bloch(z) case:

$$H_{\text{eff}} = \int d^3x\left\{\frac{\hbar}{2}(1-\cos\theta)(\partial_x\phi)\left[\frac{\Delta}{\varepsilon_F} - \frac{m}{2\Delta\hbar^2}\lambda^2\right]J - \frac{\lambda m\Delta}{\varepsilon_F\hbar}e_y J + \frac{\lambda^2 m}{\hbar^2}n_0(1-e_z)(1+\sin\phi)\right\}. \tag{65}$$

Néel(x) case:

$$H_{\text{eff}} = \int d^3x\left[\frac{\hbar}{2}(1-\cos\theta)(\partial_x\phi)\frac{\Delta}{\varepsilon_F}J - \frac{\lambda m\Delta}{\varepsilon_F\hbar}e_y J + \frac{m}{\hbar}\lambda^2(1-e_x)n_0(1+\cos^2\phi)\right]. \tag{66}$$

Bloch(y) case:

$$H_{\text{eff}} = \int d^3x\left\{\frac{\hbar}{2}(1-\cos\theta)(\partial_x\phi)\left[\frac{\Delta}{\varepsilon_F} + \frac{m}{\varepsilon_F\hbar^2}\lambda^2 + \frac{2m}{\Delta\hbar^2}\lambda^2\right]J - \frac{\lambda m\Delta}{\varepsilon_F\hbar}e_y J + \frac{m}{\hbar^2}\lambda^2 n_0[e_y + \sin^2\phi(1-e_y)]\right\}. \tag{67}$$

Here e_α is the local spin component in α direction. The first term of each effective Hamiltonian represents spin transfer torque, which is enhanced by Rashba interaction in Bloch(z)

TABLE II. Summary of effects of Rashba interaction for three configurations represented by the order of the effects in λ. Symbol × denotes the absence of the effect.

	Bloch(z)	Néel(x)	Bloch(y)
Enhancement of spin transfer torque	$O(\lambda^2)$	×	$O(\lambda^2)$
Effective magnetic field	$O(\lambda)$	$O(\lambda)$	$O(\lambda)$
Change of magnetic anisotropy	$O(\lambda^2)$	$O(\lambda^2)$	$O(\lambda^2)$

and Bloch(y) cases at the second order in spin-orbit interaction. The enhancement is thus small but independent of sign of λ. The second term of the effective Hamiltonian, $e_y\lambda\frac{\Delta}{\varepsilon_F}J$, indicates that the effective magnetic field arises in the y direction in all three cases. This is a result of spin current induced by Rashba interaction and applied current. The last term of each Hamiltonian exists without electric field and thus represents magnetic anisotropy modified by Rashba interaction. This change of magnetic anisotropy is at the second order in λ and is small. Furthermore, in reality, this static contribution should be contained already in the anisotropy parameters $K, K_\perp$. We therefore do not take it into account in the following analysis.

The effects of Rashba interaction are summarized in Table II.

VII. EQUATION OF MOTION OF DOMAIN WALL

Let us discuss how the Rashba spin-orbit interaction affects current-induced domain wall motion based on the effective Hamiltonian we derived. For this Lagrangian formalization is convenient. We consider rigid planar domain wall. The Lagrangian for domain wall is then obtained as $L=\dot{X}\phi - (H_S+H_{\rm eff})|_{X,\phi}$, where X is domain wall position, ϕ is local spin angle in magnetic easy plane, and $(H_S+H_{\rm eff})|_{X,\phi}$ is effective spin Hamiltonian evaluated for domain wall configuration.[23] Explicitly, domain wall Lagrangian is given as follows:

Bloch(z) wall:

$$\tilde{L}=[\phi\dot{\tilde{X}}-\sin^2\phi]+\cos\phi\dot{\tilde{\phi}}-\frac{\pi s^y}{2}[\tilde{\dot{X}}\cos\phi-\sin\phi\dot{\tilde{\phi}}]-s^z\tilde{X}\dot{\tilde{\phi}} - \phi\left[\frac{\Delta}{\varepsilon_F}-\frac{\hbar^2}{2\Delta m\ell^2}\tilde{\lambda}^2\right]\tilde{J}+\pi\tilde{\lambda}\sin\phi\frac{\Delta}{\varepsilon_F}\tilde{J}. \tag{68}$$

Néel(x) wall:

$$\tilde{L}=[\phi\dot{\tilde{X}}-\sin^2\phi]-s^x\tilde{X}\dot{\tilde{\phi}}+\frac{\pi s^y}{2}[\tilde{\dot{X}}\sin\phi+\cos\phi\dot{\tilde{\phi}}]-\phi\frac{\Delta}{\varepsilon_F}\tilde{J} + \pi\tilde{\lambda}\cos\phi\frac{\Delta}{\varepsilon_F}\tilde{J}. \tag{69}$$

Bloch(y) wall:

$$\tilde{L}=[\phi\dot{\tilde{X}}-\sin^2\phi]-s^y\frac{X}{\ell}\dot{\tilde{\phi}}-\phi\left[\frac{\Delta}{\varepsilon_F}+\frac{\hbar^2\tilde{\lambda}^2}{m\ell^2\varepsilon_F}+\frac{2\hbar^2\tilde{\lambda}^2}{m\ell^2\Delta}\right]\tilde{J} - 2\tilde{\lambda}\frac{X(t)}{\ell}\frac{\Delta}{\varepsilon_F}\tilde{J}.$$

Here we introduced the following dimensionless parameters:

$$\tilde{L}\equiv\frac{\ell}{\hbar NSv_c}L,\quad \tilde{X}\equiv\frac{X}{\ell},\quad \dot{\tilde{X}}\equiv\frac{\dot{X}}{v_c},\quad \dot{\tilde{\phi}}\equiv\frac{\ell}{v_c}\dot{\phi},$$

$$\tilde{J}\equiv\frac{J}{v_c},\quad \tilde{\lambda}\equiv\frac{m\ell}{\hbar^2}\lambda,$$

where N is a number of local spin in the domain wall and ℓ is the domain wall thickness given as $\ell\equiv\sqrt{\frac{J}{K}}$. (Dimensionless time is $\tilde{t}\equiv\frac{v_c}{\ell}t$.) Here a velocity $v_c\equiv\frac{K_\perp S\ell}{2\hbar}$ corresponds to drift velocity of electron at intrinsic threshold current without Rashba interaction.[23]

Equations of motion for domain wall is obtained, taking account of dissipation as $(Q=\tilde{X},\phi)$

$$\frac{\partial}{\partial\tilde{t}}\frac{\partial\tilde{L}}{\partial\dot{Q}}-\frac{\partial\tilde{L}}{\partial Q}=-\frac{\partial W_s}{\partial\dot{Q}}, \tag{70}$$

where $\tilde{W}_s$ is the dimensionless dissipation function written as $\tilde{W}_s=\frac{\alpha}{2}[\dot{\tilde{X}}^2+\dot{\tilde{\phi}}^2]$ (Ref. 25).

In deriving the equation of motion, we neglect the contribution of conduction-electron density ($s^\gamma\ll 1$) since they turn out to be small in actual situations. The equation of motion is obtained as follows:

Bloch(z) wall:

$$\dot{\tilde{X}}-\alpha\dot{\tilde{\phi}}=\sin 2\phi+\left[\frac{\Delta}{\varepsilon_F}-\frac{\hbar^2}{2\Delta m\ell^2}\tilde{\lambda}^2\right]\tilde{J}-\pi\tilde{\lambda}\cos\phi\frac{\Delta}{\varepsilon_F}\tilde{J}, \tag{71}$$

$$\dot{\tilde{\phi}}+\alpha\dot{\tilde{X}}=0, \tag{72}$$

where time evolution of ϕ reduces to a single equation of

$$\dot{\tilde{\phi}}=-\frac{\alpha}{1+\alpha^2}\left[\sin 2\phi+\left(\frac{\Delta}{\varepsilon_F}-\frac{\hbar^2}{2\Delta m\ell^2}\tilde{\lambda}^2\right)\tilde{J}-\pi\tilde{\lambda}\cos\phi\frac{\Delta}{\varepsilon_F}\tilde{J}\right]. \tag{73}$$

Néel(x) wall:

$$\dot{\tilde{X}}-\alpha\dot{\tilde{\phi}}=\sin 2\phi+\frac{\Delta}{\varepsilon_F}\tilde{J}+\pi\tilde{\lambda}\sin\phi\frac{\Delta}{\varepsilon_F}\tilde{J}, \tag{74}$$

$$\dot{\tilde{\phi}}+\alpha\dot{\tilde{X}}=0, \tag{75}$$

which result in

$$\dot{\tilde{\phi}}=-\frac{\alpha}{1+\alpha^2}\left[\sin 2\phi+\frac{\Delta}{\varepsilon_F}\tilde{J}+\pi\tilde{\lambda}\sin\phi\frac{\Delta}{\varepsilon_F}\tilde{J}\right]. \tag{76}$$

Bloch(y) wall:

$$\dot{\tilde{X}} - \alpha\dot{\tilde{\phi}} = \sin 2\phi + \left[\frac{\Delta}{\varepsilon_F} + \frac{\hbar^2\tilde{\lambda}^2}{m\ell^2\varepsilon_F} + \frac{2\hbar^2\tilde{\lambda}^2}{m\ell^2\Delta}\right]\tilde{J}, \quad (77)$$

$$\dot{\tilde{\phi}} + \alpha\dot{\tilde{X}} = -\frac{2\tilde{\lambda}\Delta}{\varepsilon_F}\tilde{J}, \quad (78)$$

and the time evolution of ϕ is obtained as

$$\dot{\tilde{\phi}} = -\frac{\alpha}{1+\alpha^2}\left[\sin 2\phi + \left(\frac{\Delta}{\varepsilon_F} + \frac{\hbar^2\tilde{\lambda}^2}{m\ell^2\varepsilon_F} + \frac{2\hbar^2\tilde{\lambda}^2}{m\ell^2\Delta}\right)\tilde{J} + \frac{2\hbar\tilde{\lambda}^2}{m\ell v_c}n_0 \sin 2\phi\frac{X}{\ell} + \frac{2}{\alpha}\frac{\tilde{\lambda}\Delta}{\varepsilon_F}\tilde{J}\right]. \quad (79)$$

Here we see a large difference between Bloch(y) and other cases. In fact, the angle ϕ in Bloch(y) wall is directly driven by current and Rashba interaction as indicated by the right-hand side of Eq. (78). Such effect of current has been known as β terms in the case of electron-spin relaxation due to random spin.[10,31] In the present Rashba case, the parameter β is then given by

$$\beta = -\frac{2\tilde{\lambda}\Delta}{\varepsilon_F}, \quad (80)$$

for Bloch(y) [$\beta=0$ for Bloch(z) and Néel(x) walls]. This result can be explained by noting that β terms is effectively equivalent to an external magnetic field and that the Rashba interaction induces an effective magnetic field, which coincides with the easy axis for Bloch(y) wall [(Eq. (67)]. We will see below that this coefficient β is quite large even assuming standard semiconducting systems; it reduces much threshold current and enhances the wall velocity. The effect would be even stronger if the systems have giant Rashba effect as realized in metallic surfaces.[8]

The effect of effective magnetic field due to Rashba interaction in Bloch(z) and Néel(x) cases is to induce anisotropy within ϕ plane as seen as cos ϕ and sin ϕ terms in Eqs. (71) and (74), respectively. This anisotropy energy turns out to drive stepwise wall motion at low current.

We also saw from Eqs. (71) and (77) that spin transfer torque effect (represented by the second term of right-hand side) is enhanced by Rashba interaction, at the second order of λ in Bloch(z) and Bloch(y) cases but not in Néel(x) case. Numerically, these second-order effects are negligibly small as we will be shown below.

VIII. DOMAIN WALL DYNAMICS

We first note that the domain wall velocity $\dot{\tilde{X}}$ is closely related to $\dot{\tilde{\phi}}$ (Ref. 23). In fact, from Eqs. (72), (75), and (78), we have seen that

$$\dot{\tilde{X}} = -\frac{1}{\alpha}\dot{\tilde{\phi}}[\text{Bloch}(z) \text{ and } \text{Neel}(x) \text{ wall}], \quad (81)$$

and

$$\dot{\tilde{X}} = -\frac{1}{\alpha}\dot{\tilde{\phi}} - \frac{2\tilde{\lambda}\Delta}{\alpha\varepsilon_F}\tilde{J}[\text{Bloch}(y) \text{ wall}]. \quad (82)$$

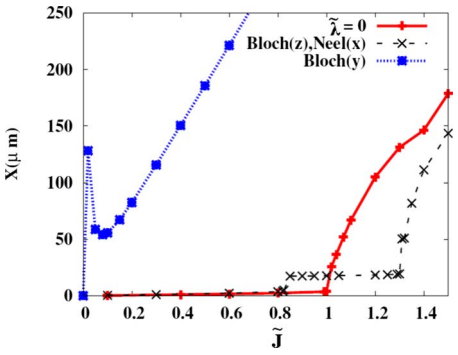

FIG. 8. (Color online) Wall position at $t=1$ μs as function of dimensionless current, $\tilde{J}=J/v_c$. Solid line represents the case $\tilde{\lambda}=0$, and dashed and dotted lines represent the case $\tilde{\lambda}=0.1$ for Bloch(z), Néel(x), and Bloch(y) walls, respectively.

Here, we showed numerical results based on the equation of motion. Parameters are chosen as

$$a = 5.65 \times 10^{-10} \text{ m}, \quad m = 0.05m_e, \quad m_e = 9.11 \times 10^{-31} \text{ kg},$$

$$v_c = 163 \text{ m/s}, \quad \varepsilon_F = 80 \text{ meV}, \quad \Delta = 40 \text{ meV},$$

$$\ell = 50 \text{ nm}, \quad \alpha = 0.01,$$

to simulate actual semiconductor systems.[9] (We thus have $\frac{\hbar^2}{m\ell^2\varepsilon_F} \simeq 0.007$, and so the second-order contribution from Rashba interaction is very small such as $\tilde{\lambda}^2\frac{\hbar^2}{m\ell^2\varepsilon_F} \simeq 0.7 \times 10^{-4}$ for $\tilde{\lambda}=0.1$.) We calculated the domain wall position $\tilde{X}(t)$ after current is applied at $t=0$.

Figure 8 shows the wall position at $t=1$ μm after current is applied. (Current is normalized by v_c, the electron drift velocity at intrinsic threshold.) The case without Rashba interaction is shown as solid line. We see here the intrinsic pinning due to hard axis anisotropy,[23] since we do not consider β term of non-Rashba origin. Wall motion in the presence of Rashba interaction with $\tilde{\lambda}=0.1$ is plotted by lines marked by $\times$ for Bloch(z) and Néel(x), and $*$ for Bloch(y) walls. Bloch(z) and Néel(x) walls behaves essentially the same.

A. Bloch(y) wall

We immediately see that Rashba interaction affects Bloch(y) wall drastically, resulting in vanishing of threshold current and of very high velocity. This is due to a large effective β term induced by Rashba interaction [Eq. (80)]. (Note that we do not consider extrinsic pinning.) For the present parameters, its ratio to α is given as $\frac{\beta}{\alpha}=\frac{\tilde{\lambda}}{\alpha}$, and so very large value of $\beta/\alpha \sim 10$ can be realized in actual experiment with $\tilde{\lambda} \sim 0.1$ and $\alpha=0.01$. Terminal wall velocity of Bloch(y) wall is plotted for different values of $\tilde{\lambda}$ in Fig. 9.

The behavior is consistent with previous studies including β term[11,12] indicating that the present motion of Bloch(y) is governed by β term induced by Rashba interaction. It is natural since β term is linear in $\tilde{\lambda}$ [Eq. (80)], while other

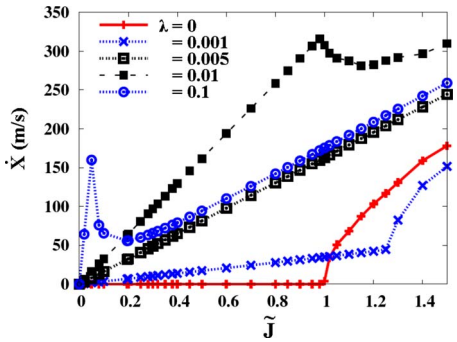

FIG. 9. (Color online) Plot of wall velocity as function is current for $\tilde{\lambda}=0$, 0.001, 0.005, 0.01, and 0.1. Damping constant is $\alpha=0.01$.

effects of Rashba interaction enter at the second order [see Eq. (77)]. Within our analysis, which neglects the extrinsic pinning, threshold current of Bloch(y) is zero due to β term. In reality, however, finite threshold will appear from pinning potential.[11,12] Due to the β term, we have obtained a very large wall velocity (such as 100 m/s) at a very small current (such as 10% of intrinsic threshold current). In reality, Gilbert damping (α) is also modified by Rashba interaction, which might slow the velocity v according to $v \propto \beta/\alpha$ (Ref. 12). The modification of α is, however, second order in λ (Refs. 32 and 33) and thus small; the high wall velocity would remain unchanged.

B. Bloch(z) and Néel(x) walls

Behaviors of Bloch(z) and Néel(x) walls are essentially the same for present values of parameters, and are distinct from Bloch(y) wall. These walls have a plateau in v-J curve for $0.8 \leq \tilde{J} \leq 1.3$ as seen in Fig. 8. This plateau is due to a step motion of wall induced by the anisotropy field within ϕ plane arising from Rashba interaction. This stepwise motion is induced above threshold current of ~0.8, and the distance the wall moves is about 22 μm regardless of current density (for $0.8 \leq \tilde{J} \leq 1.3$).

Let us see the mechanism of the plateau in detail. Dynamics near intrinsic pinning threshold is described by a potential for ϕ (Ref. 23), obtained from the Lagrangian [Eqs. (68) and (69) as follows:

Bloch(z):

$$\tilde{V}(\phi) = \sin^2 \phi + \frac{\phi}{2S}\left[\frac{\Delta}{\varepsilon_F} + \frac{\hbar^2}{2\Delta m \ell^2}\tilde{\lambda}^2\right]\tilde{J} - \frac{\pi}{2S}\tilde{\lambda} \sin \phi \frac{\Delta}{\varepsilon_F}\tilde{J}. \tag{83}$$

Néel(x):

$$\tilde{V}(\phi) = \sin^2 \phi + \frac{\phi}{2S}\frac{\Delta}{\varepsilon_F}\tilde{J} - \frac{\pi}{2S}\tilde{\lambda} \cos \phi \frac{\Delta}{\varepsilon_F}\tilde{J}. \tag{84}$$

These potentials are plotted in Fig. 10. In the absence of current, the potential is solely by magnetic anisotropy, and the energy minimum is at $\phi=0$ [Fig. 10(1)]. When current is applied, the potential tilts [Fig. 10(2)]. When local minimum

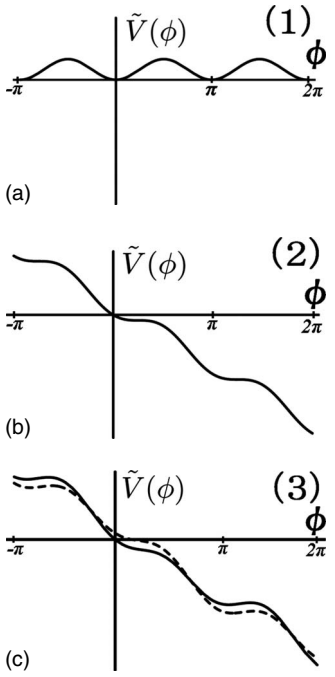

FIG. 10. Potential for ϕ of domain wall. (1) is the potential without current and Rashba interaction, namely, potential due to the hard axis anisotropy energy. Energy minimums are at $\phi=0, \pi, \ldots$ (2) includes the effect of applied current below threshold, which tilts the potential ($\tilde{J}<0$ here). (The intrinsic threshold at $\tilde{J}=1$ corresponds to the current where local minimum near $\phi \sim 0$ disappears.) (3) shows the potential in the presence of Rashba interaction, which lowers (lifts) the energy barrier around $\phi \sim \frac{\pi}{2}$ for Néel(x) shown by dashed line [Bloch(z) shown by solid line].

near $\phi=0$ vanishes, the wall starts to move and this gives the intrinsic threshold current of $\tilde{J}_c=1$ in the absence of Rashba interaction.[23] When Rashba interaction is switched, π periodicity of potential is broken due to the last terms in Eqs. (83) and (84). The way of deformation depends on Bloch(z) and Néel(x) cases. Let us consider a Néel(x) wall case where the local energy barrier around $\pi \sim \frac{\pi}{2}$ is lowered by Rashba interaction. The variable ϕ (and wall) starts to move at threshold current (where the local minimum disappears), which is lowered by Rashba interaction. But this motion stops if current is not large enough since ϕ is trapped by the next local minimum near $\phi \sim \pi$, which has a large energy barrier around $\pi \sim \frac{3\pi}{2}$. Thus in this regime, ϕ hops roughly by the amount $\Delta\phi = O(\pi)$ and this corresponds to Eq. (81) by a wall shift of $\Delta X = \frac{\ell}{\alpha}\Delta\phi$. This distance corresponds to the distance ~20 μm seen in Fig. 8. If current is sufficiently large to remove the second local minimum, the wall motion continues and the terminal velocity grows (for $\tilde{J}>1.3$ in Fig. 8). This is the mechanism of plateau.

An interesting consequence of the step motion is an asymmetric ratchet motion. We consider a Néel wall initially at $\phi=0$ (we choose $\tilde{\lambda}>0$). When we apply a negative current, $\tilde{J}<0$, the local minimum at $\phi=0$ is lifted and the energy barrier for right direction is lowered as seen in Fig. 10. In contrast, when current is positive, $\tilde{J}>0$, the local minimum

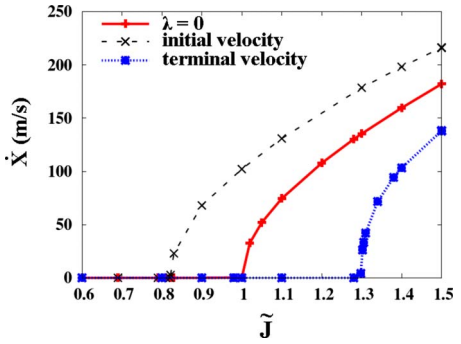

FIG. 11. (Color online) The initial and terminal velocity as function of dimensionless current in the case of Bloch(z) and Néel(x) wall. The velocity is the same for the two walls.

is lowered [$\propto -\tilde{\lambda}\tilde{J}$ by Eq. (84)] and then the effective energy barrier in the left direction becomes higher. Therefore, the threshold current for step motion differs by amount $\Delta\tilde{J}\sim\tilde{\lambda}$ for the two current directions (starting from fix ϕ), and thus, the wall behaves as a ratchet moving only in one way if current is small enough. These features are common for Bloch(z) wall case if $\phi=0$ is replaced by $\phi=\pi$.

The plateau region has finite initial velocity (but zero terminal velocity). Figure 11 shows the initial and terminal velocities for Bloch(z) and Néel(x) walls (the velocity is the same for two walls).

We see that even plateau region shows a high velocity comparable to terminal velocity above $\tilde{J}=1$. For device application, motion over a distance of 20 μm is large enough and so the plateau region would be quite useful for low current switching.

IX. CONCLUSION

We have theoretically calculated the effect of the Rashba spin-orbit interaction on the spin transfer torque. The effective Hamiltonian of local spin under current was calculated using gauge transformation, and the equation of motion for domain wall was derived. We considered three cases with different magnetic easy and hard axes, where domain wall structures realized are called Bloch(z), Néel(x), and Néel(x) walls. We found that there are three influences of Rashba spin-orbit interaction, namely, inducing effective magnetic field, increasing spin transfer torque, and modification of magnetic anisotropy. The major effect is that of effective magnetic field, which arises at the first-order in Rashba interaction. Applying voltage in x direction, the effective magnetic field is induced in y direction via Rashba interaction. In the case of Bloch(y) wall, where y direction is the easy axis direction, we showed this field acts as a force that pushes the wall, or in other words, the effective β term arises. Threshold current thus vanishes. The value of β is large even if it is evaluated for common semiconductor systems, and the wall velocity is enhanced greatly. In contrast, in the cases of Bloch(z) and Néel(x), the effective field is perpendicular to the easy axis (z and x directions, respectively), and the step motion of wall over a distance of $\Delta X\sim O(\frac{\pi\ell}{\alpha})$ arises at low current regime, corresponding to a change of the angle out of easy plane, $\Delta\phi\sim O(\pi)$. The current necessary for this step motion is lower than the case without Rashba interaction (by 20% at $\tilde{\lambda}=0.1$). The initial velocity of step motion is high enough (the same order as steady motion slightly above intrinsic threshold). Wall motion in the step motion regime is asymmetric with respect to current direction, i.e., wall behaves as a ratchet.

Other effects by Rashba interaction, modification of spin transfer torque, and anisotropy, appears at second order, $\tilde{\lambda}^2$, and are negligibly small. Change of spin transfer is due to the change of effective electron-spin polarization by Rashba interaction.

Rashba interaction arises quite generally when inversion symmetry is broken, e.g., on surface of metals doped with heavy ions.[7,8] Such systems would be suitable to realize quite high wall velocity at very small current, which we have predicted for Bloch(y).

ACKNOWLEDGMENT

The authors were grateful to H. Kohno, J. Shibata, J. Ohe, and E. Saitoh for the valuable discussion.

[1] L. Berger, J. Appl. Phys. **49**, 2156 (1978).
[2] L. Berger, Phys. Rev. B **33**, 1572 (1986).
[3] L. Berger, Phys. Rev. B **54**, 9353 (1996).
[4] J. C. Slonczewski, J. Magn. Magn. Mater. **159**, L1 (1996).
[5] E. I. Rashba, Sov. Phys. Solid State **2**, 1109 (1960).
[6] S. LaShell, B. A. McDougall, and E. Jensen, Phys. Rev. Lett. **77**, 3419 (1996).
[7] T. Nakagawa, O. Ohgami, Y. Saito, H. Okuyama, M. Nishijima, and T. Aruga, Phys. Rev. B **75**, 155409 (2007).
[8] C. R. Ast, J. Henk, A. Ernst, L. Moreschini, M. C. Falub, D. Pacilé, P. Bruno, K. Kern, and M. Grioni, Phys. Rev. Lett. **98**, 186807 (2007).
[9] M. Yamanouchi, D. Chiba, F. Matsukura, and H. Ohno, Nature (London) **428**, 539 (2004).
[10] S. Zhang and Z. Li, Phys. Rev. Lett. **93**, 127204 (2004).
[11] A. Thiaville, Y. Nakatani, J. Miltat, and Y. Suzuki, Europhys. Lett. **69**, 990 (2005).
[12] G. Tatara, T. Takayama, H. Kohno, J. Shibata, Y. Nakatani, and H. Fukuyama, J. Phys. Soc. Jpn. **75**, 064708 (2006).
[13] Y. Tserkovnyak, H. J. Skadsem, A. Brataas, and G. E. W. Bauer, Phys. Rev. B **74**, 144405 (2006).
[14] H. Kohno, G. Tatara, and J. Shibata, J. Phys. Soc. Jpn. **75**, 113706 (2006).
[15] H. Kohno and J. Shibata, J. Phys. Soc. Jpn. **76**, 063710 (2007).
[16] R. A. Duine, A. S. Nunez, J. Sinova, and A. H. MacDonald, Phys. Rev. B **75**, 214420 (2007).
[17] A. K. Nguyen, H. J. Skadsem, and A. Brataas, Phys. Rev. Lett. **98**, 146602 (2007).

[18] L. Thomas, M. Hayashi, X. Jiang, R. Moriya, C. Rettner, and S. S. P. Parkin, Nature (London) **443**, 197 (2006).
[19] L. Heyne, M. Klaui, D. Backes, T. A. Moore, S. Krzyk, U. Rudiger, L. J. Heyderman, A. F. Rodriguez, F. Nolting, T. O. Mentes, M. A. Nino, A. Locatelli, K. Kirsch, and R. Mattheis, Phys. Rev. Lett. **100**, 066603 (2008).
[20] M. Yamanouchi, D. Chiba, F. Matsukura, and H. Ohno, Nature (London) **428**, 539 (2004).
[21] M. Yamanouchi, D. Chiba, F. Matsukura, T. Dietl, and H. Ohno, Phys. Rev. Lett. **96**, 096601 (2006).
[22] M. Yamanouchi, J. Ieda, F. Matsukura, S. E. Barnes, S. Maekawa, and H. Ohno, Science **317**, 1726 (2007).
[23] G. Tatara and H. Kohno, Phys. Rev. Lett. **92**, 086601 (2004).
[24] G. Tatara, H. Kohno, J. Shibata, Y. Lemaho, and K.-J. Lee, J. Phys. Soc. Jpn. **76**, 054707 (2007).
[25] G. Tatara, H. Kohno, and J. Shibata, J. Phys. Soc. Jpn. **77**, 031003 (2008).
[26] J. I. Inoue, G. E. W. Bauer, and L. W. Molenkamp, Phys. Rev. B **70**, 041303(R) (2004).
[27] V. Korenman, J. L. Murray, and R. E. Prange, Phys. Rev. B **16**, 4032 (1977).
[28] G. Tatara and H. Fukuyama, Phys. Rev. Lett. **72**, 772 (1994); J. Phys. Soc. Jpn. **63**, 2538 (1994).
[29] L. V. Keldysh, Zh. Eksp. Teor. Fiz. **47**, 1515 (1964) [Sov. Phys. JETP **20**, 1018 (1965)].
[30] J. Rammer and H. Smith, Rev. Mod. Phys. **58**, 323 (1986).
[31] Z. Li and S. Zhang, Phys. Rev. B **70**, 024417 (2004).
[32] E. M. Hankiewicz, G. Vignale, and Y. Tserkovnyak, Phys. Rev. B **75**, 174434 (2007).
[33] H. Kohno (private communication).